ARTICLE

Nanopore Gates via Reversible Crosslinking of Polymer Brushes: A Theoretical Study

Received 00th January 20xx,
Accepted 00th January 20xx

DOI: 10.1039/x0xx00000x

Yamila A. Perez Sirkin,[a] Mario Tagliazucchi*[a] and Igal Szleifer*[b]

Polymer-brush-modified nanopores are synthetic structures inspired by the gated transport exhibited by their biological counterparts. This work theoretically analyzes how the reversible crosslinking of a polymer network by soluble species can be used to control transport through nanochannels and pores. The study was performed with a molecular theory that allows inhomogeneities in the three spatial dimensions and explicitly takes into account the size, shape and conformations of all molecular species, considers the intermolecular interactions between the polymers and the soluble crosslinkers and includes the presence of a translocating particle inside the pore. It is shown than increasing the concentration of the soluble crosslinkers in bulk solution leads to a gradual increase of its number within the pore until a critical bulk concentration is reached. At the critical concentration, the number crosslinkers inside the pore increases abruptly. For long chains, this sudden transition triggers the collapse of the polymer brush to the center of the nanopore. The resulting structure increases the free-energy barrier that a translocating particle has to surmount to go across the pore and modifies the route of translocation from the axis of the pore to its walls. On the other hand, for short polymer chains the crosslinkers trigger the collapse of the brush to the pore walls, which reduces the translocation barrier.

Introduction

The outstanding selectivity and versatility of biological systems have inspired the scientific community to attempt to mimic their behaviors in synthetic devices with similar functions. Nowadays, one of the goals is to obtain selective and stimuli-gated transport of macromolecules or nanoparticles through synthetic nanopores. In nature, the nuclear pore complex (NPC)[1–5] excels in the selectivity with which it gates the exchange of biomolecules between the cell nucleus and the cytoplasm. This biological complex allows small biomolecules to diffuse passively, but large molecules need the presence of specific transport receptors to translocate the NPC. This degree of selectivity is achieved due to the presence of disordered proteins known as FG-nucleoporins (FG-nups) that form a selective barrier inside the NPC, and soluble proteins (the nuclear transport receptors, NTRs), which bind to other proteins and grant them passage through that barrier. The mechanistic details of macromolecular transport through the NPC are still under discussion.[6–8] The formation of a reversibly crosslinked polymer network due to transient interactions between FG domains has been put forward as a potential mechanism for transport selectivity.[9,10] Notably, unbound NTRs are also present in the NPC[11–14] and are believed to contribute to the crosslinking and collapse the FG-Nups via multivalent interactions.[11,15] While the actual contribution of the described mechanism to the exceptional selectivity of the NPC is still under debate, it is interesting to ask whether reversible crosslinking of a polymer network by a soluble species can be used to control selective transport through nanochannels and nanopores.

Polymer-brush-modified nanopores inspired by the NPC were already shown to display selective and gated transport at the level of a single molecule.[16–18] The energy landscape that a particle experiences during translocation modulates the kinetics of this process. This modulation can be achieved, for example, by using a specific external stimulus that changes the interaction between polymer chains and, thus, rearranges the polymer layer within the channel from a closed to an open configuration.[19–24] Inspired by the proposed mechanism of reversible crosslinking of FG-Nups by NTRs, one can envisage a polymer-brush-modified nanopore where soluble species in solution crosslink the polymers inside the pore and trigger a structural reorganization. For example. Guo *et al.* reported a nanopore modified by ss-DNA chains that can be crosslinked into a mesh using a soluble Y-shaped DNA motif with three sticky ends.[25] Siwy and coworkers demonstrated reversible network formation in ss-DNA-modified nanochannels via proton uptake (acid-base chemistry).[26] There exists many other chemistries that can be used to crosslink polymer chains with small molecules from solution, for example metal complexation[27,28] and borate-hydroxyl reactions.[29]

Theoretical modeling has proven to be an essential tool to establish transport mechanisms and test new designs in the field of nanofluidics. The reversibly crosslinking of polymer-brush-modified nanochannels by the presence of cohesive particles has been studied before with theory and simulations.[30–34] In a related study, Lopez and Nap have

[a] *INQUIMAE-CONICET and DQIAQF, University of Buenos Aires, School of Sciences, Ciudad Universitaria, Pabellón 2, Ciudad Autónoma de Buenos Aires C1428EHA, Argentina*
[b] *Department of Biomedical Engineering, Department of Chemistry and Chemistry of Life Processes Institute, Northwestern University, Evanston, Illinois 60208, United States*

† Footnotes relating to the title and/or authors should appear here.
Electronic Supplementary Information (ESI) available: [details of any supplementary information available should be included here]. See DOI: 10.1039/x0xx00000x

theoretically explored the reversible crosslinking of a nanochannel modified by a poly(acrylate) brush with Ca^{2+} ions in solution.[35] These studies have shown that the soluble crosslinker species can collapse the polymer brush and, depending on the relation between the length of the polymer and the radius of the channel, the collapsed structure can form a compact layer on the wall or a dense plug along the channel axis. A key question that was not addressed in these previous works is to what degree this morphological transition can be used to control the translocation of large cargos (*i.e.*, nanoparticles or macromolecules with a size not much smaller than the width of the pore). This information can be obtained by calculating the free-energy landscape for the translocation of a single particle through the nanopore.[36,37] In a recent publication, we used a molecular theory to study the translocation of a nanoparticle through (uncrosslinked) polymer-brush-modified nanochannels.[36] The theoretical tool used in that study allowed inhomogeneities in the three dimensions, which -unlike previous studies-[37,38] permitted to study off-axis translocation pathways (*i.e.*, pathways where the particle does not necessarily move along the channel axis). In fact, we observed that large cargoes and cargoes having strong attractions to the brush preferentially translocated near the channel walls.

In this work, we apply a molecular theory allowing inhomogeneities in the three dimensions to study the effect of mobile crosslinkers on the conformation of polymer-modified nanopores. We explore how the change in morphology due to reversible crosslinking of the polymer brush affects the translocation of a single particle. The results are divided into two sections. In the first part, we discuss the effect of the crosslinker on the morphology of the system. For long chains (compared with the radius of the pore), we show that the theory predicts a van-der-Waals-loop type of behavior for the number of crosslinker molecules inside the pore as a function of its bulk concentration (chemical potential). This behavior suggests the presence of a sudden collapse transition beyond a critical bulk concentration of crosslinkers, which is accompanied by a collapse of the polymer brush to the axis of the pore. The theory also predicts the possible existence of metastable states, which may result in hysteresis of the properties of the pore in response to changes in the external concentration of crosslinkers. On the other hand, for short chains, the theory predicts a continuous collapse transition to the walls of the nanopore. In the second part of the manuscript, we study the effect on the collapse transition in the translocation of a single cargo. We show the crosslinker-induced collapse of the brush to the center of the pore results in an energetic barrier that shifts the translocation route from an axial pathway to a trajectory near the pore walls. In the presence of attractive interactions between the translocating cargo and the polymer, a potential-energy well develops within the pore, but the central energy barrier due to the plug persists because of its very high polymer density. In the case of short polymer brushes, which collapse to pore walls, the particle always translocates along the axis of the pore and the presence of crosslinkers decreases the height of the translocation barrier, *i.e.,* the effect is opposite to that observed for the collapsed-to-the-center morphology.

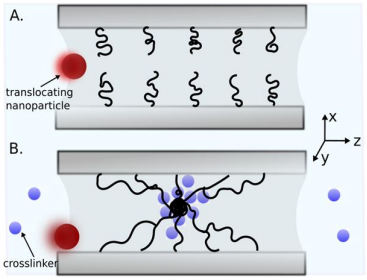

Figure 1. Schematic representation of a single nanopore modified by a crosslinkeable polymer brush. The nanopore connects two macroscopic reservoirs that contain identical solutions. A. The polymer is in good solvent conditions, therefore, in the absence of soluble crosslinking particles the brush is swollen. B. The addition of mobile crosslinker particles to the solution (small blue particles) leads to morphological transitions in the brush. The red particle translocates through the nanopore.

Theoretical methods

The system studied in this work is represented in Figure 1. A short nanopore of 5 nm radius and 17 nm length is modified with a polymer brush with a surface density of 0.075 chains·nm^{-2}. The polymer chains are homogeneously distributed on the inner walls of the pore, forming five rings with eight chains per ring. The nanopore connects two identical reservoirs that contain small soluble crosslinkers with a radius of 0.5 nm. To analyze the structural and thermodynamic properties of this system, we use a theoretical method that explicitly accounts for the size, shape, and conformations of all molecular species and their intermolecular interactions. In previous works,[36,37,39–41] similar theoretical approaches have shown excellent agreement with experiments. The starting point of the theory consists in writing down an approximate expression for the semi-grand canonical free-energy functional of the system, as shown in Eq 1.

$$\beta\Omega = \beta\mathcal{F}_{\text{trans,s}} + \beta\mathcal{F}_{\text{conf}} + \beta\mathcal{F}_{\text{trans,cl}} + \beta\mathcal{F}_{\text{cl,sp}} - \beta N_{\text{cl}}\mu_{\text{cl}} + \beta\mathcal{F}_{\text{p,sp}} \quad (1)$$

In this equation, β is $1/k_B T$, where k_B is the Boltzmann's constant and T is the temperature. The first and third terms of the right hand represent the translational entropies of the solvent and the crosslinkers, respectively:

$$\beta\mathcal{F}_{\text{trans}} = \int \rho_s(\mathbf{r})\left[\ln\left(\rho_s(\mathbf{r})v_s\right) - 1\right]d\mathbf{r} \quad (2)$$

and

$$\beta\mathcal{F}_{\text{trans,cl}} = \int \rho_{\text{cl}}(\mathbf{r})\left[\ln\left(\rho_{\text{cl}}(\mathbf{r})\nu_s\right) - 1\right]d\mathbf{r} \quad (3)$$

where $\rho_i(\mathbf{r})$ is the number density of species *i* at position **r**, and v_s is the molecular volume of the solvent. In all cases, unless it is mentioned, the integral runs over all the space that is not occupied by the translocating particle or the membrane. The second term is the conformational entropy of the polymers.

$$\beta\mathcal{F}_{\text{conf}} = \sum_{j}^{N_{chains}} \sum_{\alpha} P_P(j,\alpha)\ln\left(P_P(j,\alpha)\right) \quad (4)$$

where $P_P(j,\alpha)$ is the probability of finding the polymer chain grafted at the grafting point *j* in the system ($1 < j < N_{\text{chains}}$) in a conformation α. The fourth term represents the interaction between the polymer and the crosslinkers. This interaction is modeled as a (non-local) attractive energy given by the function $U_{\text{cl,sp}}(\mathbf{r},\mathbf{r}')$, which is the crosslinker-segment attractive energy between a crosslinker at $\mathbf{r}'$ and a segment at **r**. At a mean-field

level, this interaction results in the following contribution to the free-energy:

$$\beta\mathcal{F}_{\mathrm{cl,sp}} = \int d\mathbf{r}\left\langle n_P(\mathbf{r})\right\rangle \int d\mathbf{r}'\rho_{\mathrm{cl}}(\mathbf{r}')\beta U_{\mathrm{cl,sp}}(\mathbf{r},\mathbf{r}') \quad (5)$$

where $\left\langle n_P(\mathbf{r})\right\rangle$ is the average density of polymer segments at **r**, and it calculated as

$$\left\langle n_P(\mathbf{r})\right\rangle = \sum_{j}^{N_{chains}} \sum_{\alpha} P_P(j,\alpha) n_P(j,\alpha,\mathbf{r}) \quad (6)$$

where $n_P(j,\alpha,\mathbf{r})d\mathbf{r}$ is the number of segments that the chain *j* in the system has in the volume element between **r** and **r** + d**r** when it is in conformation α.
In this work, we used a square-well potential for $U_{\mathrm{cl,sp}}(\mathbf{r},\mathbf{r}')$:

$$U_{cl,sp}(\mathbf{r},\mathbf{r}') = -\epsilon_{cl,sp} \quad \text{if } |\mathbf{r}\text{-}\mathbf{r}'| < \delta$$
$$U_{cl,sp}(\mathbf{r},\mathbf{r}') = 0 \quad \text{elsewhere} \quad (7)$$

where we used δ = 0.5 nm. Note that other types of interaction could have been used to model the segment-polymer crosslinking process, such as a chemical-reaction formalism,[35,42,43] which is best suited when the crosslinking process follows a well-defined stoichiometry. However, in this work we are not modeling any specific interaction and, therefore, we opted to model the crosslinker-segment interaction using eqs. (5) and (7). This expression is simpler and, in our experience, easier to implement and solve than the chemical reaction formalism. Moreover, other types of interaction potential could also have been used instead of the square-well. Once again, we chose this potential based on its simplicity, its small number of parameters, and its short range (which accelerates calculations).

The fifth contribution to Ω is the $-N_{cl}\mu_{\mathrm{cl}}$ term that is required because the functional is grand canonical with respect to the crosslinkers,

$$-\beta\mu_{\mathrm{cl}}N_{cl} = -\beta\mu_{\mathrm{cl}}\int \rho_{\mathrm{cl}}(\mathbf{r})d\mathbf{r} \quad (8)$$

The last term is the interaction energy of the translocating particle and polymer segments:

$$\beta\mathcal{F}_{\mathrm{p,sp}} = \int \left\langle n_P(\mathbf{r})\right\rangle \beta U_{\mathrm{p,sp}}(\mathbf{r},\mathbf{R})d\mathbf{r} \quad (9)$$

where $U_{\mathrm{p,sp}}$ represents the particle-segment energy, which we also model with a square-well potential with a depth $\varepsilon_{\mathrm{p,sp}}$, and thickness δ:

$$U_{p,sp}(\mathbf{r},\mathbf{R}) = -\epsilon_{p,sp} \quad \text{if } |\mathbf{r}\text{-}\mathbf{R}| < \delta$$
$$U_{p,sp}(\mathbf{r},\mathbf{R}) = 0 \quad \text{elsewhere} \quad (10)$$

The repulsions in the system are modelled as excluded-volume interactions for segments, crosslinkers, and solvent molecules. This contribution is treated exactly for intrachain segment-segment repulsions by considering only polymer conformations that are self-avoiding. It is also exactly accounted for the interaction of solvent molecules, crosslinkers and chain segments with pore walls and the translocating particle. For all other interactions in the system, the excluded volume interaction is modelled as a packing constraint, which holds for all points of the space that are not part of the translocating particle or the pore walls:

$$\rho_s(\mathbf{r})v_s + \left\langle\phi_P(\mathbf{r})\right\rangle + \left\langle\phi_{\mathrm{cl}}(\mathbf{r})\right\rangle = 1 \quad (11)$$

where

$$\left\langle\phi_P(\mathbf{r})\right\rangle = \left\langle n_P(\mathbf{r})\right\rangle v_P \quad (12)$$

with v_{p} is the volume of a polymer segment and $\langle\phi_{\mathrm{cl}}(\mathbf{r})\rangle$ is the volume fraction of the crosslinkers:

$$\left\langle\phi_{\mathrm{cl}}(\mathbf{r})\right\rangle = \int \rho_{\mathrm{cl}}(\mathbf{r}')\nu_{\mathrm{cl}}(\mathbf{r},\mathbf{r}')d\mathbf{r}' \quad (13)$$

the integral over **r**′ takes into account the contribution to the volume at **r** from crosslinkers everywhere and $v_{\mathrm{cl}}(\mathbf{r},\mathbf{r}')d\mathbf{r}$ is the volume that a crosslinker with its center at **r**′ has in the volume element between **r** and **r** + d**r**.

We emphasize that the packing constraint, Eq.(11), applies only to regions that are not part of the pore walls or the translocating particle. In this way, the translocating particle is explicitly modelled as an impenetrable object in the theory. On the other hand, the crosslinker particles (which are smaller than the translocating particle) are considered as a density field.[44–47]

Another constraint used to minimize the semi-grand canonical free energy is the normalization of the probability-distribution function of the polymer chains,

$$\sum_{\alpha} P_P(j,\alpha) = 1 \quad \text{for all } j \quad (14)$$

These constraints are taken into account using Lagrange multipliers. Therefore, the function to minimize is *W*,

$$W = \Omega + \int \pi(\mathbf{r})\left[\rho_s(\mathbf{r})v_s + \left\langle\phi_P(\mathbf{r})\right\rangle + \left\langle\phi_{\mathrm{cl}}(\mathbf{r})\right\rangle - 1\right]d\mathbf{r} + \sum_{j}^{N_{chains}} \eta(j)\left[\sum_{\alpha} P_P(j,\alpha) - 1\right] \quad (15)$$

where π(**r**) and η(*j*) are the Lagrange multipliers associated with the packing constraint and the normalization of the probability distribution function of chain conformations, respectively. The equilibrium condition is obtained from the minimum of *W* respect to $\rho_s(\mathbf{r})$, $\rho_{\mathrm{cl}}(\mathbf{r})$ and $P_P(j,\alpha)$.

The minimum of *W* respect to $\rho_s(\mathbf{r})$ leads to the following equation:

$$\rho_s(\mathbf{r}) = \frac{1}{v_s}\exp\left[-\beta\pi(\mathbf{r})v_s\right] \quad (16)$$

It is possible to take the value in the bulk as a reference

$$\rho_s^{\mathrm{bulk}} = \frac{1}{v_s}\exp\left[-\beta\pi^{\mathrm{bulk}}v_s\right] \quad (17)$$

therefore,

$$\rho_s(\mathbf{r}) = \rho_s^{\mathrm{bulk}}\exp\left[-\beta v_s\left(\pi(\mathbf{r}) - \pi^{\mathrm{bulk}}\right)\right] \quad (18)$$

The minimum of *W* respect to $\rho_{\mathrm{cl}}(\mathbf{r})$, after some rearrangements, leads to:

$$\rho_{\mathrm{cl}}(\mathbf{r}) = \frac{1}{v_s}\exp\left[\beta\mu_{cl} - \int \beta\pi(\mathbf{r}')v_{\mathrm{cl}}(\mathbf{r}',\mathbf{r})d\mathbf{r}' - \int \langle n_P(\mathbf{r}')\rangle\beta U_{cl,sp}(\mathbf{r}',\mathbf{r})d\mathbf{r}'\right] \quad (19)$$

the bulk reference is

$$\rho_{\mathrm{cl}}^{\mathrm{bulk}} = \frac{1}{v_s}\exp\left(\beta\Delta\mu_{cl}\right) \quad (20)$$

where we defined:

$$\Delta\mu_{cl} = \mu_{cl} - \pi^{bulk}v_{cl}^{total} = \ln\left(\rho_{cl}^{bulk}\right) \quad (21)$$

and $v_{\mathrm{cl}}^{\mathrm{total}}$ is the total volume of the crosslinker.

Combining Eqs. (19) and (20), results in:

$$\rho_{\rm cl}(\mathbf{r}) = \rho_{\rm cl}^{\rm bulk}\exp\Big[-\beta\Big(\int\pi(\mathbf{r}')v_{\rm cl}(\mathbf{r}',\mathbf{r})d\mathbf{r}' - \pi^{\rm bulk}v_{cl}^{total}\Big) - \int\big\langle n_P(\mathbf{r}')\big\rangle\beta U_{cl,sp}(\mathbf{r}',\mathbf{r})d\mathbf{r}'\Big] \quad (22)$$

The minimum of W respect to $P_P(j,\alpha)$ is

$$P_P(j,\alpha) = \frac{1}{\xi(j)}\exp\Big\{-\int n_P(j,\alpha,\mathbf{r})\big[v_P\beta\pi(\mathbf{r}) + \int\rho_{\rm cl}(\mathbf{r}')\beta U_{cl,sp}(\mathbf{r},\mathbf{r}')d\mathbf{r}' + U_{p,sp}(\mathbf{r},\mathbf{R})\big]d\mathbf{r}\Big\} \quad (23)$$

The equations of the theory are discretized in the three dimensions *x*, *y*, *z*, with a discretization step of Δ = 0.5 nm. Note that some of the discretized cubic sites are part nanopore wall or translocating particle and part solution or polymer. In order to properly model these cells, we define a mask function $f_v(\mathbf{r})$, where $f_v(\mathbf{r})$ = 0 when the point **r** is part of the nanopore or the translocating particle, and $f_v(\mathbf{r})$ = 1 when it is part of the solution or polymer layer. Therefore, the average volume fraction of a cell that is occupied by the solution is computed as:

$$\overline{f_v}(i) = \frac{1}{\Delta^3}\int_{\rm cell\ i} f_v(\mathbf{r})d\mathbf{r} \quad (24)$$

where the integration runs over the cell *i*, and Δ is the volume of the discretized cube.

Equations (17) and (22) are discretized as:

$$\rho_s(i) = \rho_s^{\rm bulk}\exp\big[-\beta v_s\big(\pi(i) - \pi^{\rm bulk}\big)\big] \quad (25)$$

,and

$$\rho_{\rm cl}(i) = \rho_{\rm cl}^{\rm bulk}\exp\left[-\beta\left(\sum_j\pi(j)\nu_{\rm cl}(j,i) - \pi^{\rm bulk}v_{\rm cl}\right) - \sum_j\big\langle n_P(j)\big\rangle\overline{U}_{\rm cl,sp}(j,i)\overline{f_v}(j)\Delta^3\right] \quad (26)$$

respectively, where $\bar{U}_{\rm cl,sp}(j,i)$ is the average interaction of a mobile crosslinker at cell *i* with polymer segments at cell *j*, and it is given by

$$\overline{U}_{cl,sp}(j,i) = \frac{1}{\Delta^3}\int_{\rm cell\ j} U_{cl,sp}(\mathbf{r}',\mathbf{r}(i))d\mathbf{r}' \quad (27)$$

where **r**(*i*) is the center of cell *i*.

Eq. (23) is discretized to:

$$P_P(j,\alpha) = \frac{1}{\xi(j)}\exp\left\{-\sum_k n_P(j,\alpha,k)\big[v_P\beta\pi(k) + \sum_i\overline{U}_{\rm cl,sp}(k,i)\rho_{\rm cl}(i)\overline{f_v}(i)\Delta^3 + \overline{U}_{p,sp}(j,\mathbf{R})\big]\right\} \quad (28)$$

where $n_P(j,\alpha,k)$ is the number of segments that a chain grafted at position *j* has in the conformation α in the cell *k* , and

$$\overline{U}_{p,sp}(j,\mathbf{R}) = \frac{1}{\Delta^3}\int_{\rm cell\ j} U_{p,sp}(\mathbf{r},\mathbf{R})f_v(\mathbf{r})d\mathbf{r} \quad (29)$$

The discretized packing constraint, Eq. (11), is

$$\rho_s(i)v_s + \big\langle\phi_P(i)\big\rangle + \big\langle\phi_{\rm cl}(i)\big\rangle = 1 \quad (30)$$

where

$$\big\langle n_P(i)\big\rangle = \sum_j^{N_{chains}}\sum_\alpha P_P(j,\alpha)n_P(j,\alpha,i) \quad (31)$$

To solve the molecular theory, we first generate the self-avoiding polymer conformations (*i.e.*, the matrix $n_P(j,\alpha,i)$) using a rotational isomeric state model[48,49] and a random sampling procedure. We solve Eqs. (25)-(31) using a Jacobian Free Newton Method implemented in the numerical library Sundials Kinsol.[50] In this procedure, the unknown variables $x(i)$ are the densities of the solvent and the polymer segments, $\rho_s(i)$ and $\langle n_P(i)\rangle$ respectively, in each grid site; therefore, we have $2N_{cells}$ unknown, where N_{cells} is the number of cells in the system. In each iteration of the solver, trial $\rho_s(i)$ and $\langle n_P(i)\rangle$ values are first used to calculate $\pi(i)$ from Eq. (25), $\rho_{\rm cl}(i)$ using Eq. (26) and $P_P(j,\alpha)$ with Eq. (28). The packing constraint and the definition of $\langle n_P(i)\rangle$, Eqs. (30) and (31), are set equal to zero to form a set of $2N_{\rm cells}$ equations $F(i) = 0$, and the trial values calculated above are replaced into these equations to calculate $F(i)$. The numerical solver iterates $x(i)$ until the sum residuals is below a target tolerance.

Results and Discussions

Morphology

We first studied the effect of the bulk density of the crosslinkers on the behavior of the system. Figures 2A, B, and C show the polymer density within the pore for a chain length of 30 segments per chain, good solvent conditions for the polymer, and an interaction between the polymer segments and the crosslinkers of 2.0 k_BT. In the absence of crosslinkers (or in the presence or a small number of them), the polymer brush has a swollen conformation (Figure 2A). As the concentration of crosslinkers in solution increases, the number of crosslinkers inside the pore ($N_{\rm cl}$) also increases and leads to an effective attraction between polymer chains. Once the number of crosslinkers inside the pore reaches a certain value, there is a transition to a collapsed structure, which we call a central plug (Figures 2B and 2C). Another type of central plug was observed in previous works, but it was triggered by increasing the interaction between polymer chains (*i.e.,* in a poor solvent for the polymer).[23,39,51] We emphasize that in the present work, the polymer chains are in good solvent conditions and they experience effective attractions only because of the presence of crosslinker particles inside the pore. Figures 2D, 2E, and 2F show the number density of crosslinkers for the same systems of Figures 2A, 2B, and 2C, respectively. It can be observed that the spatial distributions of the crosslinkers and the polymer segments are very similar. Based on this observation, we will show only the polymer distributions in the following analysis.

For a specific design of the nanopore, the partition of crosslinkers between the reservoir and the pore depends on the chemical nature of the crosslinker. In our model, the properties of the crosslinker are determined by the strength of its interaction with the polymer segments, $\varepsilon_{\rm cl,sp}$ (see Eq. (7)), and its size, which we fix to 0.5 nm in radius. Figure 3A shows the bulk density of the crosslinkers as a function of their number inside the pore (same conditions as Figure 2). It is important to clarify two aspects related to this plot. First, the bulk density of crosslinkers depends on their chemical potential in the system, $\Delta\mu_{\rm cl}$ (see Eq. (21)); therefore the two variables plotted in Figure 3A (number of crosslinkers inside the pore and crosslinker bulk density) are thermodynamically conjugated variables. The

second aspect to mention is that the bulk density of crosslinkers is actually the experimentally controllable variable, but we plot it in the y-axis of Figure 3A to stress the presence of a van-der-Waals loop, which indicates that we are in the presence of a transition.

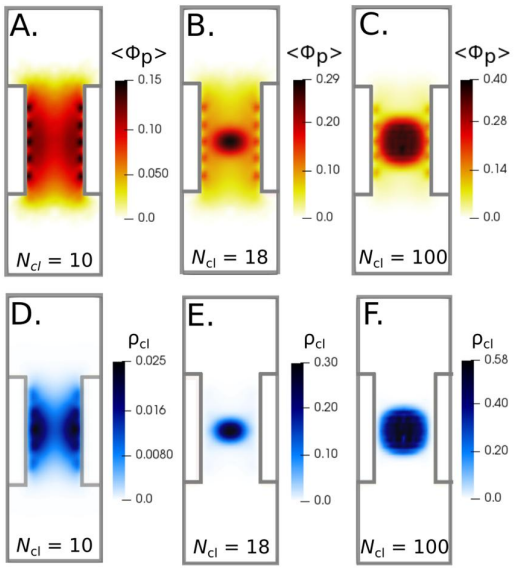

Figure 2: A-C. Color maps of the volume fraction of the polymer along a longitudinal cut of the pore (*x*-*z* plane) for pores having a different total number of crosslinkers (N_{cl}). D-F. Color maps of the number density of crosslinkers (units of particles/nm^3) in the same condition as A to C, respectively. The distributions of the polymer and the crosslinker in the space are similar. It can be observed a transition from a non-collapsed structure to a central plug when the number of crosslinkers increases (note that different panels use different color scales).

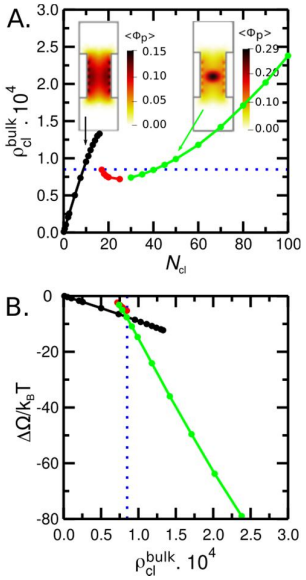

Figure 3: A. Bulk number density of crosslinkers (units of crosslinkers/nm^3) versus the total number of crosslinkers inside the pore. The black, red, and green lines represent the different behaviors of the system. The system exhibits a transition from a non-collapsed structure for the black line to a central-plug morphology for the green line. The insets show color maps of the volume fraction of the polymer for both regions. B. Semi-grand canonical free energy of the system, $\Delta\Omega$, versus the number density of crosslinkers. The three regions shown in panel A are presented with the same color in B. In both plots, the blue dotted line shows the bulk density of crosslinkers when the swollen and central plug morphologies have the same $\Delta\Omega$.

The plot in Figure 3 shows three well-defined regions with different dependencies of the bulk density with the total number of crosslinkers. The black line shows the behavior of the system starting from zero crosslinkers. As expected, increasing the bulk density leads to an increase in the total number of crosslinkers inside the pore. As shown in the color map in the inset of Figure 3A, in this region the number of crosslinkers inside the pore is not large enough to modify the brush morphology. For a value of $N_{cl} \sim 19$ crosslinkers/pore, the slope of the ρ_{cl}^{bulk} vs N_{cl} becomes negative (red line). Since ρ_{cl}^{bulk} vs N_{cl} are thermodynamically conjugated variables, this negative slope indicates that the system is not thermodynamically stable in this region. For $N_{cl} > 25$ crosslinkers/pore, the system becomes thermodynamically stable again. In this region, the polymer brush inside the pore is strongly collapsed to the central axis due to the presence of the crosslinkers.

The van-der-Waals loop in Figure 3A suggests that upon increasing the bulk density of the crosslinker, ρ_{cl}^{bulk}, the system will undergo a sudden transition from a swollen state with low N_{cl} (black curve) to a collapsed state with large N_{cl} (green curve). The equilibrium value of ρ_{cl}^{bulk} for the transition will be the one where the grand free-energies of these two states become equal. Figure 3B represents the grand free energy of the system as a function of the crosslinker bulk density. The three regions are represented with the same colors as in Figure 3A. The crossover between the black and green lines shows the density where both structures have the same free energy, and, therefore, the collapse transition is expected. A similar behavior was observed in the previous work of Osmanovic *et al.*,[30] where calculations from a classical density functional theory with azimuthal symmetry suggested that colloid particles can switch the system from a wall phase to the central-plug morphology. The authors proposed that this change is compatible with a transition from an open to a close configuration, although the energetics of particle translocation was not explored.

We constructed state diagrams for the system for different chain lengths, N_{seg}, and strengths of the crosslinker-segment interaction, $\varepsilon_{cl,sp}$. In Figure 4A, the black lines indicate points in the $\Delta\mu_{cl}$ vs N_{cl} plane where the collapsed and swollen structures have the same grand free energy and the same chemical potential of crosslinkers (*i.e.,* points corresponding to the crossing of black and green lines in Figure 3B). In the region between the red dashed lines in Fig. 4A, $\Delta\mu_{cl}$ decreases with N_{cl}, and, therefore, the system is thermodynamically unstable. In the region located between each red dashed line and black solid line, $\Delta\mu_{cl}$ increases with N_{cl} and, therefore, the structure with the highest grand free energy may exist as a metastable structure. For a macroscopic system, the black and red lines would indicate the "binodal" and "spinodal" of the transition. At this point, we should stress that our system is not a thermodynamic phase and, therefore, the concepts of binodal and spinodal, derived for macroscopic phase equilibria, should be used with care. Thus, the results in Figure 4A can be interpreted in different ways. It can be argued that there is no possible analogy between a macroscopic phase coexistence and our nanoscopic system. In that situation, the region between the red dashed curves is thermodynamically forbidden. Therefore, increasing the bulk density of crosslinkers can gradually increase their number inside the pore until reaching

the red dashed line (assuming that the system stays as a metastable state between the black and the red dashed line). Any further increase of the bulk density will necessarily trigger the collapse of the brush and produce a discontinuous jump of the number of crosslinkers inside the pore (N_{cl} would jump from one red dashed line to the other). An alternative interpretation of our results consists in imagining an ensemble of pores instead of only one. In that interpretation, N_{cl} in the axis of Figure 4A will correspond to an average value. In this interpretation, the ensemble of pores may exist in the region between the red dashed lines provided that some pores are swollen and have a small N_{cl} and others are collapsed and have a large N_{cl}.

Note that a critical point is not observed in Fig. 4A due to the fact that the number of segments in the polymer chain, N_{seg}, can only be increased by integer values (the critical point should be between 17 < N_{seg}^{crit} < 18). Moreover, even when the effect of a continuous parameter is studied (*e.g.*, $\varepsilon_{cl,sp}$), it is necessary a very fine sampling of the phase space near the critical point to locate it, which makes this task a computationally expensive one. In principle, starting with different initial configurations it may be possible to access the metastable region in an experiment, *i.e.*, we expect some degree of hysteresis in this system. Another interesting observation, is that the number of crosslinkers inside the pore, N_{cl}, required to trigger the transition experiences a minimum with respect to the chain length (black lines in Fig. 4A). We attribute this behavior to the fact that long polymers can collapse easier than short ones due to their flexibility. On the other hand, short polymers require fewer crosslinkers than long ones to achieve a given crosslinker:segment ratio. We believe that this tradeoff between the crosslinker:segment stoichiometry and the polymer flexibility is the origin of the minimum of the N_{cl} required for the transition with respect to the chain length.

Figure 4B shows the same information as in Figure 4A, but in the $\Delta\mu_{cl}$ vs N_{seg} (number of segments per chain) plane. The red line shows the equilibrium condition between the swollen and the collapsed conformation (*i.e.,* the crossing of the green and black lines in Figure 3A). Increasing the number of segments per chain favors the collapse of the layer via the incorporation of soluble crosslinkers. Therefore, in Figure 4B, increasing N_{seg} decreases the bulk density of crosslinkers required for the transitions (*i.e.*, it decreases $\Delta\mu_{cl}$).

The morphology of the collapsed structure depends on the relation between N_{seg} and the radius of the nanopore.[23] The insets in Figure 4B show color maps for the volume fraction for the different conformations of the polymer brush. As we discussed above for long polymers (N_{seg} > 17), the brush collapses to the center of the pore upon increasing N_{cl}. On the other hand, for N_{seg} < 17, a collapsed-to-the-wall conformation is observed (see inset in the upper left corner of Figure 4B). This result is in line with previous MD simulations for a similar system to that discussed here, which have shown a close-to-open transition due to the presence of nanoparticles.[32] In that transition, the polymer brush switched from an extended morphology in the closed state to a collapsed-to-the-wall layer in the open pore. As a conclusion, by changing the relation between the radius of the nanopore and the length of the polymer chains and adjusting the polymer-crosslinker interaction, it is possible to obtain different collapsed structures. Another interesting observation is that the collapse-to-the-walls transition is a continuous (*i.e.,* it does not involve a van-der-Waals loop like the formation of the central plug). This difference may be related to the fact that the collapse-to-the-center mechanism requires a change in the radial redistribution of the polymer density because the region of the highest polymer volume fraction shifts from the pore walls to the pore axis upon collapse. On the contrary, in the collapse-to-the-wall mechanism, the symmetry of the polymer distribution is preserved.

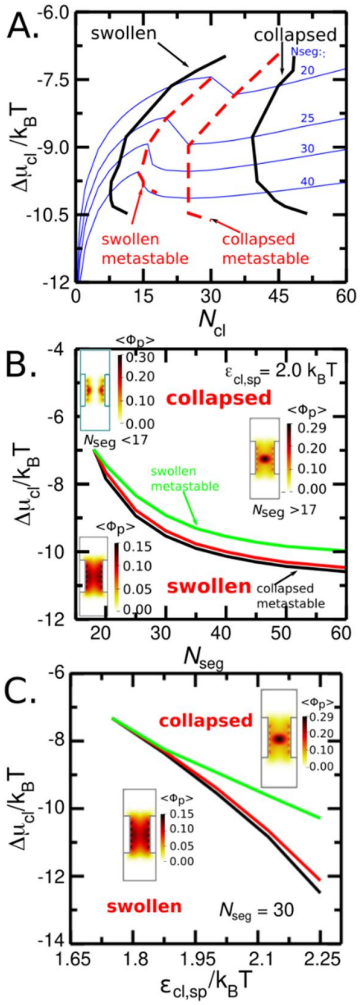

Figure 4. A. State diagram of the system in the $\Delta\mu_{cl} = ln(\rho_{cl}^{bulk})$ (chemical potential of crosslinkers) vs N_{cl} (number of crosslinkers inside the pore) plane. Each blue curve correspond to a different chain length of the polymer, N_{seg}, as it is indicated in the figure. For all curves, $\epsilon_{cl,sp} = 2.0\ k_BT$. The black lines indicate the values of N_{cl} at points where the swollen and collapsed states have the same grand free energy (crossing of black and green lines in Figure 3B). The region delimited by the red dashed lines corresponds to a thermodynamically unstable system (number of crosslinkers decreasing with their chemical potential). B. Same results as in A, but plotted in the $\Delta\mu_{cl} = ln(\rho_{cl}^{bulk})$ vs N_{seg} plane. C. Same plot as B, but for fixed N_{seg} = 30 and different values of $\varepsilon_{cl,sp}$. The insets in B and C show color maps for the density of polymer segments for typical examples of each morphology.

In Figure 4C we show the same plot as Figure 4B, but for different strengths of the crosslinker-segment interaction, $\epsilon_{cl,sp}$, and fixed N_{seg} = 30. As expected, decreasing the strength of the interaction favors the swollen morphology, for which the entropic contributions to the free energy dominates over the enthalpic segment-crosslinker attractions. Therefore, the bulk density of crosslinkers required for the transition (and thus $\Delta\mu_{cl}$) decreases with increasing $\epsilon_{cl,sp}$. The insets in this figure show examples of stable conformations in each region.

It is interesting to remark that for bulk densities of crosslinkers where both the swollen and collapsed structures are possible, these two structures exhibit a different number of crosslinkers inside the pore. Therefore, to switch from one structure to the other, it is necessary to change the number of crosslinkers within the nanopore. Our theoretical description only allows us to predict the free energies of these structures and, therefore, equilibrium structures. It does not provide any information about the transition pathway between them (such information may be obtained in the future by using a minimum-free energy pathway formalism.[52])

Effect of Crosslinker-Induced Collapse on Cargo Translocation

By solving the molecular theory for fixed particle positions, we can compute the free-energy landscape that the particle experiences inside the pore. If we further assume that the timescale of polymer and crosslinker reorganization is much faster than that the motion of the translocating particle, then we can decouple both processes and the free-energy landscape obtained by fixing the translocating particles at different positions inside the pore can be used to predict the route of translocation. Therefore, depending on the shape of the resulting landscape, it is possible to predict information of the translocation process by looking at the presence of free-energy barriers along the minimum free-energy pathway (MFEP, *i.e.*, the translocation pathway that has the smallest barrier). In this way, if the MFEP presents a free-energy barrier similar to or smaller than the thermal energy (k_BT), one expects efficient particle translocation. In the opposite case, the particles will not be able to complete all the way through the nanopore.

In this article, we studied how the presence of crosslinkers affects the translocation of a single particle through the nanopore. In Figure 5, we present different free-energy profiles for the translocation of a single particle with neutral interaction with polymer segments ($\epsilon_{p,sp}$ = 0 k_BT, see eq. (10)) and a radius of 2 nm. Figures 5A and 5C show the free energy profile for the translocation of the nanoparticle through a pathway along the central axis of the pore (Fig. 5A) or close to its wall (Fig. 5C). In particular, in both figures, the red line represents the grand free energy of the system without crosslinkers and the black line show results when the number of crosslinkers inside the pore (in the absence of the translocating particle) is N_{cl} = 100. A comparison of the height of the free-energy barriers in both plots shows that the MFEP in the absence of crosslinkers occurs along the axis of the nanopore. In the presence of crosslinkers, the MFEP shifts and becomes close to the walls.

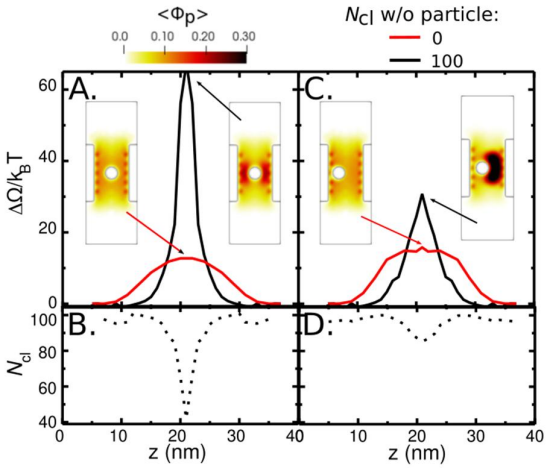

Figure 5. A, C. Grand-free-energy profiles for the translocation of a single particle with neutral polymer-particle interactions ($\epsilon_{p,sp}$ = 0 k_BT) and a radius of 2 nm. The plots show the grand free energy of the system as a function of the *z* position of the particle, *y* = 0, and values of *x* that correspond to translocation pathways along the pore axis (A) and near the pore wall (C), respectively (see the coordinate system in Figure 1). The red and black lines indicate systems without and with crosslinkers, respectively (in the latter case, N_{cl} = 100 when the translocating particle is absent). The insets in the Figure show color maps of the polymer volume fraction. B, D. Number of crosslinkers inside the pore (N_{cl}) vs z position of the translocating particle for the results in panels A and C. The polymers have a chain length of N_{seg} = 30.

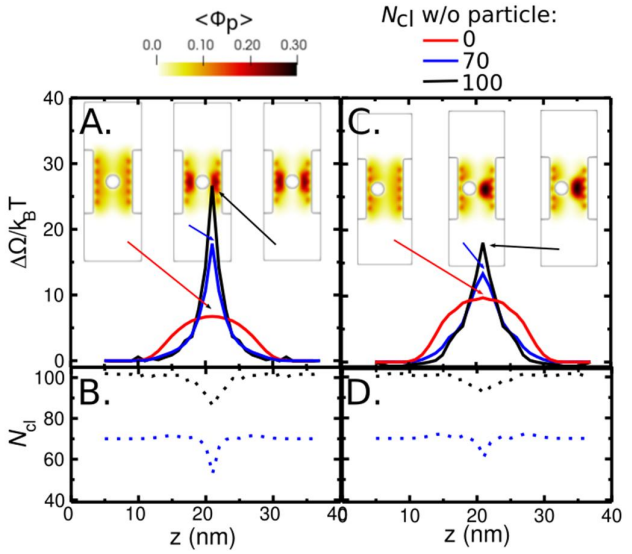

Figure 6: Same as Figure 5 but for a chain length of N_{seg} = 19. The red, blue, and black lines correspond to cases where the nanopore has N_{cl} = 0, 70, and 100 crosslinkers, respectively, in the absence of the translocating particle.

In all cases, the translocation of the 2 nm particle is energetically forbidden because the barrier is at least ~13 times larger than the thermal energy (k_BT). Nevertheless, the barrier in the presence of crosslinkers is significatively larger than that without crosslinkers. The insets in Figures 5A and 5C show the density of the polymer at the maximum of the profile. Note that for the translocation near the pore axis (Fig. 5A), the particle forces the central aggregate to split in two. Therefore, this route has larger free energy than that near the wall (Fig 5C), where the central plug has to shift to accommodate the particle, but it retains its integrity.

Figures 5B and D show that during the translocation of the particle the total number of crosslinkers inside the pore, N_{cl}, decreases when the grand free energy of the system increases. This result emphasizes the coupling between the total number of crosslinkers and the morphology of the polymer brush. Note that the decrease in the number of crosslinkers is maximum when the particle translocates through the axis of the pore. In these conditions, the central plug is split in half due to the presence of the particle and this process requires a noticeable reduction of the number of crosslinker species in the polymer layer.

The barriers in Figure 5 are too large to allow the passage of the translocating particle, both in the absence and in the presence of crosslinkers. We explored the possibility of decreasing these barriers by reducing the length of the polymer segments (N_{seg}) and the number of crosslinkers inside the nanopore (N_{cl}). In Figure 6, we present results for a shorter chain (N_{seg} = 19) than that used in Figure 5 (N_{seg} = 30). The results in this figure are qualitatively similar to those in Figure 6, but a significant decrease in the barrier is observed, for example, in the case where the number of crosslinkers is 100 (in the absence of the translocating particle), the barrier increases from ~30 k_BT for N_{seg} = 30 (black curve in Fig. 5C) to ~19 k_BT for N_{seg} = 19 (black curve in Fig. 6C, in both cases considering the translocation near the wall). Reducing the number of crosslinkers to 70 per nanopore, lowers the barrier to ~14 k_BT (blue curve in Fig. 6C). On the other hand, in the absence of crosslinkers, translocation is predicted to occur along the central axis of the pore and has a barrier of ~7 k_BT (red curve in Fig. 6A). In summary, for N_{seg} = 19, there is a large increase in the barrier upon the introduction of the crosslinkers (from ~7 k_BT to ~14-19 k_BT), but the barrier in the absence of crosslinker (~7 k_BT) is still high.

A further reduction of the length of the polymer to N_{seg} = 15, leads to a transition from a collapsed-to-the-center to a collapsed-to-the-walls morphology in the presence of crosslinkers, see insets in Fig. 4B. Figure 7 shows results for the translocation for this polymer length. The red and blue lines represent the grand free energy of the system when the total numbers of crosslinkers (in the absence of the translocating particle) are N_{cl} = 0, and 100, respectively. Interestingly, the effect of the crosslinkers on the height of the barrier is exactly opposite to that observed for the pore with a central plug in Figures 5 and 6: the barrier lowers from 3.4 k_BT in the absence of crosslinkers to 1 k_BT in their presence. Therefore, in the latter condition, particle translocation is enabled. Also, in the example in Fig. 7, the route of translocation is not modified by the collapse of the brush and it always occurs through the axis of the nanopore.

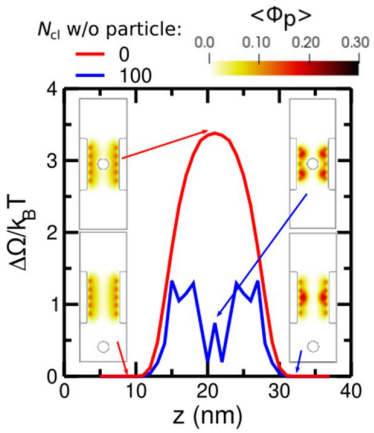

Figure 7. Grand-free-energy profiles for the translocation along the axis of the pore (which corresponds to the MFEP) of a single particle with neutral polymer-particle interaction ($\epsilon_{p,sp}$ = 0 k_BT) and a radius of 2 nm. The polymers have a chain length of N_{seg} = 15. The red, and blue lines correspond to cases where the nanopore has N_{cl} = 0, and 100 crosslinkers, respectively (in the absence of the translocating particle). The insets show the color maps of the polymer volume fraction, the left ones correspond to the red line, while the right ones to the blue line.

In all results presented above for pores with a central polymer plug (Figures 5 and 6), the barriers for translocation were always much larger than k_BT. In addition of decreasing the length of the polymer, the barrier for translocation can also be decreased by introducing an attractive interaction between the translocating particle and the polymer mesh, *i.e.*, by changing the nature of the translocating particle (or the polymer). In Figure 8, we show the effect of the strength of the attraction between the translocating particle and polymer segments, $\epsilon_{p,sp}$, on the grand free energy of the system along the MFEP for a fixed chain length of N_{seg} = 30. The dotted and solid lines show the profiles in the absence and in the presence of crosslinkers (N_{cl} = 100 without particle), respectively. The insets in Figure 8 show the position of the particle and a color map of the volume fraction of the polymer at the middle plane of the pore. As it is explained in Figure 5, the MFEP switches from the axis of the pore to close to its walls upon the introduction of the soluble crosslinkers. Upon increasing the strength of the attraction between the translocating particle and the polymer, the free-energy along the MFEP evolves from a repulsive potential (results in Fig. 5 and Fig. 8A) to an attractive one (Fig. 8B). Interestingly, the attraction between the translocating particle and the polymer does not completely remove the barrier, but rather decreases it and creates two potential wells at the entrances of the pore. Note that the well-barrier-well potential can also occur in the absence of crosslinkers (this case was studied in detail in our previous publication[36]), but the shape of the potential becomes very pronounced in the present case because of the presence of the central polymer plug, which creates a high and narrow free-energy barrier. The presence of a well could be unfavorable for translocation because the particle can get trapped. In other words, in order to translocate the nanopore, the particle would need to overcome a barrier equal to the depth of the well.

For the system without crosslinkers and $\epsilon_{p,sp}$ = 0.5 k_BT (dotted line in Fig. 8A), the translocation is possible because the

MFEP has a flat, barrierless profile. On the other hand, for the same system with crosslinkers, the translocation will be prohibited due to the presence of a barrier of ~15 k_BT. Therefore, in this case, it is possible to switch from an open to a close state due to the presence of crosslinkers.

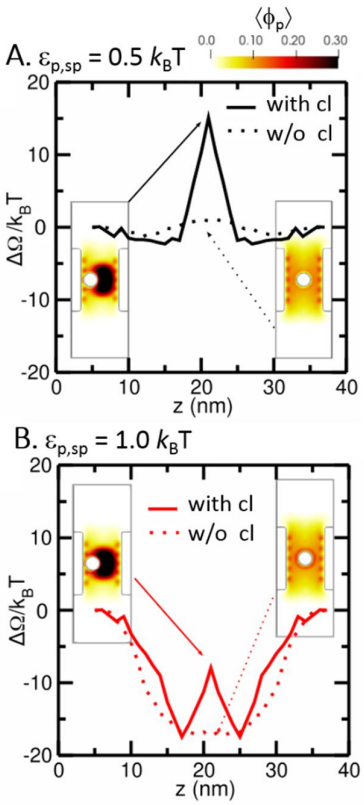

Figure 8. Free energy profiles for the translocation of a single nanoparticle of 2 nm of the radius and different interaction strengths with the segments of the polymer, $\epsilon_{p,sp}$. The solid lines and dotted lines indicate a pore in the presence (N_{cl} = 100 without translocating particle) and in the absence of crosslinkers, respectively. The insets show color maps of the volume fraction of the polymer when the nanoparticle is in the middle of the nanopore along the z coordinate. The polymers have a chain length of N_{seg} = 30.

Conclusions

We studied a nanopore modified with a neutral polymeric brush in the presence of small mobile nanoparticles in solution that are attracted to the polymer and can crosslink it. As the number of crosslinkers inside the pore increases, the polymers, which are in good solvent conditions, experience an effective attraction. Beyond a critical bulk density of crosslinkers, the polymer layer switches from a swollen conformation to a collapsed structure. We characterized the structural and thermodynamical properties of this collapse transition and studied how it is affected by the length of the polymer chains and the strength of the crosslinker-polymer attractions. We also studied the translocation of a particle much larger than the crosslinkers through the pore. The fully 3D representation of the system used in this work was crucial to take into account all possible pathways for translocation, in contrast to previous models[37,38] that assumed rotational symmetry and, therefore, were limited to the translocation route along the pore axis.

The model studied in this present work contains just the minimal elements (in terms of intermolecular interactions) required to observe the collapse transition of the polymer brush induced by the soluble crosslinkers. We believe, however, that some of its predictions may be relevant for the NPC, which is a considerably more complex system. Microscopy experiments[53] have suggested that cargo translocation across the NPC involves a double-well potential (same shape as that in Fig. 8B), which produces a pooling mechanism. In this mechanism, the cytoplasmic well increases the probability of having the cargo-kap complexes near the barrier, while the wall itself provides transport selectivity.[53] The double-well potential is not an unique feature of the central-plug morphology discussed here because we previously observed this potential in a swollen brush.[36] However, the central plug produces sharper and more defined wells and barrier than those previously observed in the absence of collapse.

Our predictions can be also useful to design synthetic nanopores with a permeability tunable by the presence of crosslinkers in solution. The most interesting result in this regard is the fact the crosslinkers can either lower or boost the barrier when the polymer chains are long or short compared with the radius of the pore, respectively. This effect arises from the existence of two possible collapse mechanisms: the collapse-to-the-center and collapse-to-the-walls scenarios.[39] The possibility of taking advantage of these two collapse mechanisms for controlling transport has been discussed in previous theoretical[22,23] and experimental works[24,54] for polymer and polyelectrolyte brushes in poor-solvent conditions.

An interesting future direction is to explore how interactions that were not included in the present simple model (electrostatic interactions, short-range hydrophobic interactions, hydrogen bonding, chemical equilibria, etc.) can affect our results. Along these lines, a long-term goal is to incorporate the presence of nuclear transport receptors in an experimentally informed, realistic model of the NPC.[55] Such model will contribute to our understanding of the role of these soluble proteins within the lumen of the NPC and may inspire new synthetic devices mimicking its outstanding transport selectivity.

Conflicts of interest

There are no conflicts to declare.

Acknowledgements

MT is a fellow of CONICET. MT acknowledges financial support from Agencia Nacional de Promoción Científica y Tecnológica (ANPCyT) PICT-0154-2016 and PICT 4649-2018 and University of Buenos Aires (UBACYT 20020170200215BA). I.S. acknowledges support from NSF, Div. of Chem. Bioeng. Env. and Transp. Sys. 1833214.

Notes and references

1 J. Fernandez-Martinez and M. P. Rout, *Curr. Opin. Cell Biol.*, 2012, **24**, 92–99.
2 S. J. Kim, J. Fernandez-Martinez, I. Nudelman, Y. Shi, W. Zhang, B. Raveh, T. Herricks, B. D. Slaughter, J. A. Hogan and P. Upla, *Nature*, 2018, **555**, 475–482.
3 O. Peleg and R. Y. Lim, *Biol. Chem.*, 2010, **391**, 719–730.
4 D. Görlich and I. W. Mattaj, *Science*, 1996, **271**, 1513–1519.
5 R. Peters, *Bioessays*, 2009, **31**, 466–477.
6 T. Jovanovic-Talisman and A. Zilman, *Biophys. J.*, 2017, **113**, 6–14.
7 R. Y. H. Lim, B. Huang and L. E. Kapinos, *Nucleus*, 2015, **6**, 366–372.
8 G. J. Stanley, A. Fassati and B. W. Hoogenboom, *Semin. Cell Dev. Biol.*, 2017, **68**, 42–51.
9 K. Ribbeck and D. Görlich, *EMBO J.*, 2001, **20**, 1320–1330.
10 S. Frey and D. Görlich, *Cell*, 2007, **130**, 512–523.
11 L. E. Kapinos, R. L. Schoch, R. S. Wagner, K. D. Schleicher and R. Y. Lim, *Biophys. J.*, 2014, **106**, 1751–1762.
12 L. E. Kapinos, B. Huang, C. Rencurel and R. Y. H. Lim, *J. Cell Biol.*, 2017, **216**, 3609–3624.
13 A. R. Lowe, J. H. Tang, J. Yassif, M. Graf, W. Y. Huang, J. T. Groves, K. Weis and J. T. Liphardt, *eLife*, 2015, **4**, e04052.
14 D. Görlich, F. Vogel, A. D. Mills, E. Hartmann and R. A. Laskey, *Nature*, 1995, **377**, 246–248.
15 R. L. Schoch, L. E. Kapinos and R. Y. Lim, *Proc. Natl. Acad. Sci.*, 2012, **109**, 16911–16916.
16 S. W. Kowalczyk, L. Kapinos, T. R. Blosser, T. Magalhães, P. van Nies, R. Y. H. Lim and C. Dekker, *Nat. Nanotechnol.*, 2011, **6**, 433–438.
17 G. Emilsson, Y. Sakiyama, B. Malekian, K. Xiong, Z. Adali-Kaya, R. Y. H. Lim and A. B. Dahlin, *ACS Cent. Sci.*, 2018, **4**, 1007–1014.
18 T. Jovanovic-Talisman, J. Tetenbaum-Novatt, A. S. McKenney, A. Zilman, R. Peters, M. P. Rout and B. T. Chait, *Nature*, 2009, **457**, 1023–1027.
19 A. Andrieu-Brunsen, S. Micoureau, M. Tagliazucchi, I. Szleifer, O. Azzaroni and G. J. Soler-Illia, *Chem. Mater.*, 2015, **27**, 808–821.
20 B. Yameen, M. Ali, R. Neumann, W. Ensinger, W. Knoll and O. Azzaroni, *Small*, 2009, **5**, 1287–1291.
21 L. Wu, J. J. Willis, I. S. McKay, B. T. Diroll, J. Qin, M. Cargnello and C. J. Tassone, *Nature*, 2017, **548**, 197.
22 K. Speyer and C. Pastorino, *Soft Matter*, 2019, **15**, 937–946.
23 Y. A. Perez Sirkin, I. Szleifer and M. Tagliazucchi, *Macromolecules*, 2020, **53**, 2616–2626.
24 O. Schepelina and I. Zharov, *Langmuir*, 2007, **23**, 12704–12709.
25 W. Guo, F. Hong, N. Liu, J. Huang, B. Wang, R. Duan, X. Lou and F. Xia, *Adv. Mater.*, 2015, **27**, 2090–2095.
26 S. F. Buchsbaum, G. Nguyen, S. Howorka and Z. S. Siwy, *J. Am. Chem. Soc.*, 2014, **136**, 9902–9905.
27 J. Brassinne, C.-A. Fustin and J.-F. Gohy, *J. Inorg. Organomet. Polym. Mater.*, 2013, **23**, 24–40.
28 N. Holten-Andersen, M. J. Harrington, H. Birkedal, B. P. Lee, P. B. Messersmith, K. Y. C. Lee and J. H. Waite, *Proc. Natl. Acad. Sci.*, 2011, **108**, 2651–2655.
29 Y. Guan and Y. Zhang, *Chem. Soc. Rev.*, 2013, **42**, 8106–8121.
30 D. Osmanović, I. J. Ford and B. W. Hoogenboom, *Biophys. J.*, 2013, **105**, 2781–2789.
31 M. G. Opferman, R. D. Coalson, D. Jasnow and A. Zilman, *Langmuir*, 2013, **29**, 8584–8591.
32 D. Ando, R. Zandi, Y. W. Kim, M. Colvin, M. Rexach and A. Gopinathan, *Biophys. J.*, 2014, **106**, 1997–2007.
33 R. D. Coalson, A. Eskandari Nasrabad, D. Jasnow and A. Zilman, *J. Phys. Chem. B*, 2015, **119**, 11858–11866.
34 A. Eskandari Nasrabad, D. Jasnow, A. Zilman and R. D. Coalson, *J. Chem. Phys.*, 2016, **145**, 064901.
35 L. G. Lopez and R. J. Nap, *Phys. Chem. Chem. Phys.*, 2018, **20**, 16657–16665.
36 M. Tagliazucchi, K. Huang and I. Szleifer, *J. Phys. Condens. Matter*, 2018, **30**, 274006.
37 M. Tagliazucchi, O. Peleg, M. Kröger, Y. Rabin and I. Szleifer, *Proc. Natl. Acad. Sci.*, 2013, **110**, 3363–3368.
38 M. Tagliazucchi, Y. Rabin and I. Szleifer, *ACS Nano*, 2013, **7**, 9085–9097.
39 O. Peleg, M. Tagliazucchi, M. Kröger, Y. Rabin and I. Szleifer, *ACS Nano*, 2011, **5**, 4737–4747.
40 M. Tagliazucchi, X. Li, M. Olvera de la Cruz and I. Szleifer, *ACS Nano*, 2014, **8**, 9998–10008.
41 K. Huang and I. Szleifer, *J. Am. Chem. Soc.*, 2017, **139**, 6422–6430.
42 R. J. Nap and I. Szleifer, *J. Chem. Phys.*, 2018, **149**, 163309.
43 G. Zaldivar and M. Tagliazucchi, *ACS Macro Lett.*, 2016, **5**, 862–866.
44 V. V. Ginzburg, *Macromolecules*, 2017, **50**, 9445–9455.
45 K. Hur, R. G. Hennig, F. A. Escobedo and U. Wiesner, *Nano Lett.*, 2012, **12**, 3218–3223.
46 V. Ganesan and A. Jayaraman, *Soft Matter*, 2014, **10**, 13–38.
47 M. Tagliazucchi and I. Szleifer, *J. Am. Chem. Soc.*, 2015, **137**, 12539–12551.
48 M. Rubinstein and R. H. Colby, *Polymer physics*, Oxford University Press New York, 2003, vol. 23.
49 P. Flory and M. Volkenstein, *Statistical mechanics of chain molecules*, Wiley Online Library, 1969.
50 A. C. Hindmarsh, P. N. Brown, K. E. Grant, S. L. Lee, R. Serban, D. E. Shumaker and C. S. Woodward, *ACM Trans. Math. Softw. TOMS*, 2005, **31**, 363–396.
51 D. Osmanović, M. Kerr-Winter, R. Eccleston, B. Hoogenboom and I. Ford, *J. Chem. Phys.*, 2015, **142**, 034901.
52 I. Gleria, E. Mocskos and M. Tagliazucchi, *Soft Matter*, 2017, **13**, 2362–2370.
53 L.-C. Tu, G. Fu, A. Zilman and S. M. Musser, *EMBO J.*, 2013, **32**, 3220–3230.
54 J. Zhang, N. Liu, B. Wei, X. Ou, X. Xu, X. Lou and F. Xia, *Chem. Commun.*, 2015, **51**, 10146–10149.
55 K. Huang, M. Tagliazucchi, S. H. Park, Y. Rabin and I. Szleifer, *Biophys. J.*, 2020, **118**, 219–231.

TOC Image